

# Variable Rate Compression for Raw 3D Point Clouds

Md Ahmed Al Muzaddid and William J. Beksi

**Abstract**—In this paper, we propose a novel variable rate deep compression architecture that operates on *raw* 3D point cloud data. The majority of learning-based point cloud compression methods work on a downsampled representation of the data. Moreover, many existing techniques require training multiple networks for different compression rates to generate consolidated point clouds of varying quality. In contrast, our network is capable of explicitly processing point clouds and generating a compressed description at a comprehensive range of bitrates. Furthermore, our approach ensures that there is no loss of information as a result of the voxelization process and the density of the point cloud does not affect the encoder/decoder performance. An extensive experimental evaluation shows that our model obtains state-of-the-art results, it is computationally efficient, and it can work directly with point cloud data thus avoiding an expensive voxelized representation.

**Index Terms**—RGB-D Perception; Deep Learning for Visual Perception; Big Data in Robotics and Automation

## I. INTRODUCTION

Among various data modalities such as audio, image, text, etc., 3D data in the form of point clouds constitutes a growing portion of the spectrum. Sensors for capturing 3D point cloud data such as light detection and ranging (LiDAR), stereo, structured light, and time-of-flight (ToF) have become increasingly popular and economical. In comparison to images, high-dimensional information can be described in 3D with immunity to variations in color, illumination, and scale. Besides point clouds, there are numerous ways to depict 3D data including meshes, CAD models, and volumetric representations. However, when compared to the other data representations, point clouds offer the advantage of providing a simpler, denser, and closer-to-reality description [1].

A point cloud consists of an unordered set of points where each point has a Cartesian coordinate value in Euclidean space. Additional attributes may include the color (i.e., RGB value) and surface normal associated with each point. Robotics is at the forefront of utilizing point clouds created by 3D sensor technology. Portrayal of the environment provided by these sensors can facilitate 3D learning-based tasks like object/scene reconstruction, motion planning and navigation, object detection and classification, pose estimation, grasp detection, etc. [2]. Other pertinent applications where point clouds are widely used include augmented and virtual reality, cultural heritage, geographical information systems, self-driving vehicles, and many more [3].

3D sensors generate enormous amounts of point cloud data at high frame rates. For example, a 3D point cloud

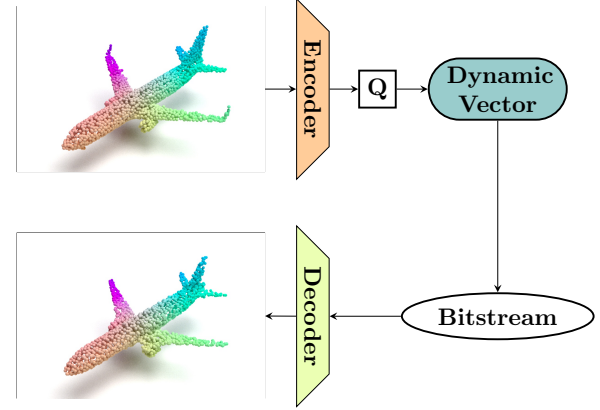


Fig. 1. 3D point clouds produced by LiDAR, stereo, structured light, and ToF sensors require a large amount of memory capacity. The transfer of point clouds to and from machines necessitates compression of the data. Our approach can reconstruct dense point clouds from a highly-compressed representation, at variable bitrates, using a single trained model.

with 0.7 million points per frame at 30 frames per second needs a bandwidth of approximately 500 MB/s for video [4]. Working with uncompressed point cloud data can lead to congestion and delays in communication networks [5]. Thus, efficient compression coding technologies are indispensable for ensuring the compact storage and transmission of such data. There exists an array point cloud compression techniques in the literature which are primarily based on the use of octrees and 2D-projection. Nevertheless, a number of deep learning-based point cloud compression methods have emerged which offer performance improvements over traditional methods.

Even though most machine learning point cloud compression research has been inspired by the success of learning-based image compression [6], there are fundamental differences between these two domains. Unlike a traditional 2D image, the structure of a 3D point cloud is irregular. Dealing with unordered 3D points is a significant dilemma. For instance, proven techniques such as convolutional layers that extract features in the image domain can not be plainly applied to raw point clouds. These 2D and 3D convolution operators are suitable for grid-like data structures. Therefore, point clouds are typically voxelized whereby points are represented as a binary occupancy cell. Although this provides a representation suitable for use with a convolutional layer, it also introduces a number of difficulties (e.g., computing and memory overhead, loss of information, etc.).

The authors are with the Department of Computer Science and Engineering, University of Texas at Arlington, Arlington, TX, USA. Emails: mdahmedal.muzaddid@mavs.uta.edu, william.beksi@uta.edu.

To address these limitations, we propose a model that can compress raw point clouds without converting them into a voxelized representation, Fig. 1. There are two prominent benefits of our approach: (i) there is no loss of information due to voxelization; (ii) the compression and reconstruction performance is not affected by the underlying point cloud density. At the same time, our technique reduces the unnecessary computational burden induced by the processing of unoccupied voxels. In summary, our contributions are the following.

- We introduce a weighted entropy loss function and inference strategy to compress point clouds at different bitrates using a single trained model.
- Our architecture eliminates the need to train multiple models for a range of bitrates thus benefiting a diversity of applications.
- We establish raw 3D point cloud compression benchmarks for a variety of tasks on publicly available datasets.

Our source code is available at [7].

The remainder of this paper is organized as follows. Relevant related literature is discussed in Section II. Our approach for variable rate deep 3D point cloud compression is presented in Section III. The design and results of our experiments are demonstrated and explained in Section IV. In Section V, the paper is concluded and future work is discussed.

## II. RELATED WORK

### A. Tree Structure-Based Compression

Octrees provide an efficient way of representing point clouds through the partitioning of space [8]. An octree-based representation builds a tree data structure that starts from the root node, where a node represents a 3D bounding box, and recursively subdivides the space into eight child nodes until a desired depth is reached. Conventional octree-based coding methods [9, 10, 11, 12, 13, 14] directly exploit the spatial correlations among points via this data structure.

Other types of tree-based representations, such as k-d trees [15] and spanning trees [16], can achieve analogous results for lossless coding [17, 18, 19]. The Moving Picture Experts Group (MPEG) has published a geometry-based point cloud compression standard (MPEG V-PCC) based on an octree data structure [20, 21]. In addition, the Point Cloud Library [22] provides octree-based implementations for point cloud compression.

### B. Projection-Based Compression

Projection-based approaches follow the principle of converting a 3D point cloud into 2D images by projection or mapping [23, 24, 25, 26, 27, 28]. Usually, the output of the projection step is represented as a set of depth images based on multiple dissimilar viewpoints or canonical planes. This provides a regular grid structure of the points, which are further partitioned into a set of patches or point clusters. Subsequent steps compress the patches using well-known image/video codecs such as JPEG [29] and HEVC [30]. The

main challenge with this technique is to find an optimum set of transformations from the 3D point set to the corresponding 2D representation. A combination of octree and projection-based methods [31] is also possible as well.

### C. Learning-Based Compression

Learning-based methods typically exploit the same transform-based coding principles used in conventional lossy image coding such as JPEG. Most of the learning-based models search for an optimum nonlinear transformation in terms of rate distortion trade-off during training time by using an appropriate differentiable objective function. For instance, the estimated entropy of a quantized latent vector can be used along with the reconstruction loss in an objective function [32, 33]. Within the image domain, convolutional neural networks (CNNs) are used to extract the translation-invariant features that encapsulate spatial correlations among neighboring pixels. Inspired by the success of CNN layers [34], complementary approaches have been adopted in learning-based point cloud compression [35, 36, 37, 38, 39].

After converting a raw point cloud into a regular voxel grid, autoencoder-based machine learning models may be used to extract a latent representation which is then quantized. The quantized latent representation is further processed by a decoder to reconstruct the point cloud. The whole model can then be trained end-to-end to optimize both reconstruction loss and entropy loss. Due to the non-differentiable nature of the quantization step, special treatment is needed inside a conventional autoencoder structure. For example, [40] carried out nearest neighbor assignments to compute the quantized value of the latent vector which relied on (differentiable) soft quantization. Motivated by theoretical links to dithering, [41] proposed to replace quantization by additive uniform noise. [42] used a stochastic rounding operation in the forward pass, while in the backward pass the derivative is replaced with the derivative of the expectation.

## III. VARIABLE RATE DEEP COMPRESSION

Our unified architecture directly takes raw point clouds as input, Fig. 2. A PointNet-based [43] feature extractor is utilized for processing point cloud data as follows. The encoder transforms a point cloud  $x$  using a parametric analysis transform,  $g_a(x; \theta_a)$ , into a latent representation  $y$ . The latent representation is then quantized to produce  $\hat{y}$ . On the receiving side, the decoder recovers  $\hat{y}$  from the compressed signal. A synthesis transformer function,  $g_s(\hat{y}; \theta_s)$ , uses  $\hat{y}$  to recover the reconstructed point cloud  $\tilde{x}$ .  $\theta_a$  and  $\theta_s$  are the weight parameters of the encoder and decoder, respectively.

Our goal is to derive uncorrelated global and local features from the point cloud input. To do this, we propose a deep learning-based approach to extract structural features from 3D data. Transforms (e.g., discrete cosine transform (DCT) [44]) have been used for decades to represent 2D image and video data in a more condensed format. Although we employ a feature extractor that encodes low-level features into compact vector representations, floating-point vectors are not suited for sending and receiving over a transmission

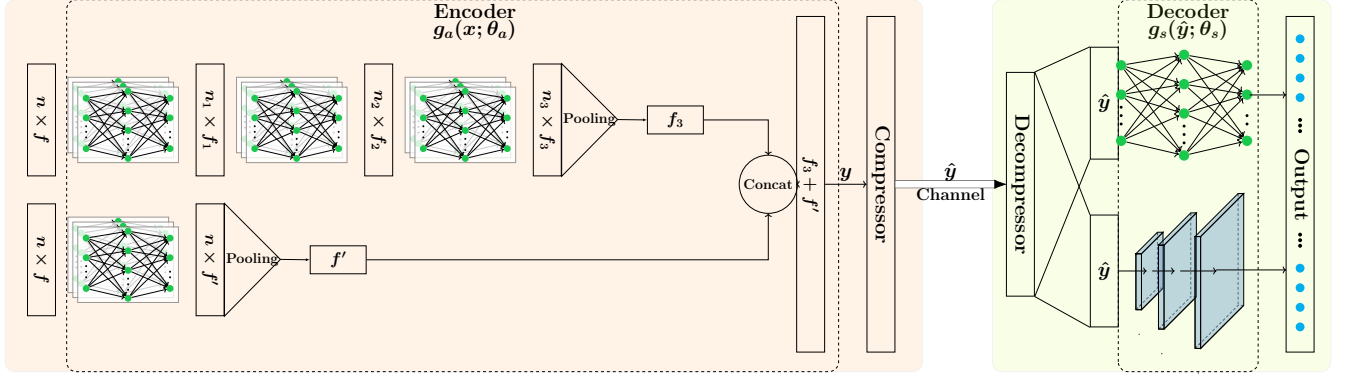


Fig. 2. An overview of our variable rate deep compression model for compressing raw 3D point clouds. The input to the model is an  $n \times f$  matrix, where  $n$  is the number of sample points and  $f$  is number of features per point. The top and bottom branches of the encoder correspond to the local and global feature extractors, respectively. At the first level in the local feature extractor, the set abstraction (SA) layer transforms the per point input features into combined features of size  $n_1 \times f_1$ . These combined features are then processed by the next level SA layer. All of the features are combined into a single feature vector of size  $f_3$  at the last level SA layer. The bottom branch converts per point input features of size  $n \times f$  into transformed features of size  $n \times f'$ . Next, a pooling operation combines the features into a single feature vector of size  $f'$ . Lastly, the two feature vectors of size  $f_3$  and  $f'$  are concatenated and processed by the compressor. The decoder first decompresses the compressed vector into  $\hat{y}$  which is then processed by both of the decoding branches (top and bottom) to produce approximately  $n$  points in total.

channel in an efficient way. This is due to the fact that precise floating-point data requires a high bitrate to transmit.

To reduce the bitrate, we further quantize the embedded vector using an adaptive quantizer coupled with a probability density model. The probability density model is applied to estimate the bitrate required to compress the quantized vector representation. A fully-connected decoder is used as a synthesis transformer to decode the quantized latent features into the reconstructed point cloud. The reconstructed point cloud is then compared against the input point cloud and the reconstruction loss is calculated. The whole model is trained end-to-end to simultaneously optimize reconstruction loss and bitrate. In the following subsections, we describe each component of the model.

### A. 3D Transform

Within the image domain, transformations are used to express data in a consolidated form. Learned 2D transforms have demonstrated improved coding performance in image compression [45, 34, 46]. A learned transform usually performs better than a traditional transform such as the DCT. This is due to the ability of the learned transform to allocate more or less bits for contrasting parts of an image based on the rate distortion constraints it is trained on. For point cloud data, a transform is typically learned via a convolutional autoencoder which takes a voxelized occupancy grid as input.

Instead of using a convolution-based feature extractor, we opt for a fully-connected layer-based feature extractor. Concretely, we use two parallel branches in our encoder module. One branch handles the global structure of the point cloud and the other branch focuses on local patterns along the disparate levels of granularity. In the global feature extractor branch, we apply a multilayer perceptron network to every point. The network weights are shared among all the points. A global feature vector is then derived by applying a symmetric function on the transformed features.

In the local feature extractor branch, features are aggregated in a hierarchical fashion to capture the geometric structure of the neighboring point cloud distribution. The points are sampled based on an iterative farthest point strategy [47] and used as keypoints to extract nearby local structure. Similar to a CNN, sampled features only focus on a small neighborhood within the initial layers. At the higher layers, features are captured at larger scales. This is comparable to the increasing receptive field size within the deeper layers of a CNN. Both feature vectors from the local and global branch are then concatenated and passed through fully-connected layers which combine them into a single latent vector  $y$ .

### B. Quantization

After obtaining the latent representation, we perform a quantization step at compression time based on the desired target quality or rate. During training, to ensure differentiability we model the discretization using additive uniform noise [45]. More formally, we define

$$q(\tilde{y} | x, \theta_s) = \prod_i U\left(\tilde{y}_i | y_i - \frac{1}{2}, y_i + \frac{1}{2}\right), \quad (1)$$

where  $\tilde{y}$  is the noisy approximation,  $U$  denotes a uniform distribution centered on  $y_i$ , and  $i \in [1, \dots, l]$  where  $l$  is the length of  $y$ . During compression, the elements of  $y$  are quantized by rounding to the nearest integer.

### C. Rate-Distortion Modeling

Following quantization, the latent vector becomes discrete-valued. Consequently, it can be compressed losslessly using entropy coding techniques such as arithmetic coding [48]. The compressed code can then be transmitted as a sequence of bits. On the receiving end, the decoder recovers the 3D coordinates from the compressed latent vector to reconstruct

the original point cloud. Given an approximate distribution  $P_{\hat{y}}$  of the quantized vector  $\hat{y}$ , we calculate the bitrate as

$$R = E_x[-\log P_{\hat{y}}(Q(g_a(x; \theta_a)))], \quad (2)$$

where  $Q$  represents the quantization function. The distortion is the expected difference between the reconstructed point cloud  $\hat{x}$  and the inceptive point cloud  $x$  as measured by a suitable distance metric. To control the rate distortion trade-off we use a traditional formulation in which an equilibrium is found between the code length and the distortion. Formally, we minimize the combined loss,  $L = D + \lambda R$ , where  $D$  is the distortion and  $\lambda$  acts as a hyperparameter that balances the two competing objectives.

#### D. Decoder

Given a vector decompressed by the decompressor, the decoder module regresses the 3D coordinate values of the point cloud. To support variable bitrates, we use a weighted entropy loss function. Through the use of variable weights for individual vector elements, we gradually reduce the importance of the elements occurring at positions later on in the compressed vector. More precisely,

$$R_{weighted} = E_x \left[ \sum_i -\omega_i \log P(\hat{y}_i) \right], \quad (3)$$

where

$$\omega_i = ae^{-b \times i} \quad (4)$$

is an exponential decaying function for assigning the  $i$ -th weight to each element in the compressed vector.

With this weighted entropy loss the overall loss function becomes  $L = D + \lambda R_{weighted}$ . During the reconstruction phase, elements appearing towards the end of the vector contribute less to the overall reconstruction. As a result, we can ignore the latter part of the vector if we have a tight budget on the bitrate. This allows us to train a single model that produces variable bitrates. We show the relation between the effective bitrate versus the reconstruction loss through a broad experimental assessment (Section IV).

### IV. EXPERIMENTAL EVALUATION

#### A. Datasets, Training, and Runtime Details

We make use of the ShapeNet [49] and ModelNet40 [50] datasets for our experimental evaluation. ShapeNet is composed of 16,881 objects from 16 classes and 50 parts in total. In addition, the category label for each object is provided. Each point cloud contains 2,048 points uniformly sampled from the surface of an object. The sampled point clouds are normalized with zero mean and scaled to a unit sphere. ModelNet40 consists of 12,311 CAD-generated objects (e.g., airplane, car, plant, lamp, etc.) from 40 categories. Within ModelNet40, 9,843 objects are used for training while the rest (2,468) are reserved for testing.

Our model was trained in batches where each sample consists of  $n = 2048$  points. Only the  $x, y, z$  coordinates are considered as input features (i.e.,  $f = 3$ ) akin to [43]. For the local feature extractor branch, three SA layers were

Task	Time (msec)		
	Batch size of 32	Batch size of 16	Batch size of 1
Compression	8.50 $\pm$ 0.10	8.60 $\pm$ 0.10	15.20 $\pm$ 0.40
Decompression	0.40 $\pm$ 0.01	0.50 $\pm$ 0.02	2.30 $\pm$ 0.10

TABLE I

ELAPSED WALL-CLOCK TIMES FOR 3D POINT CLOUD COMPRESSION AND DECOMPRESSION TASKS AVERAGED OVER TEN TRIAL RUNS.

used. The number of sampling points in each SA layer are  $n_1 = 512$ ,  $n_2 = 128$ ,  $n_3 = 1$ , and the number of features are  $f_1 = 256$ ,  $f_2 = 512$ ,  $f_3 = 512$ . In the global feature extractor branch the number of features is  $f' = 512$ . On the decoder side, we used a small fully-connected neural network of size  $512 \times 512 \times 1024$ . Max pooling was utilized for all pooling operations.

Using the Adam [51] optimizer, our network was trained for 300 iterations with an initial learning rate 0.0001, a batch size of 16, momentum value of 0.9, and momentum2 value of 0.999. Training took place on a CentOS 7.6.1810 machine using an Intel Xeon E5-2620 2.10 GHz CPU, 132 GB of memory, and an NVIDIA GeForce GTX 1080 Ti GPU. It took approximately 23 hours to train our model. All experimental tests were performed using a Ubuntu 18.04 machine with an Intel Core i7-8700 3.20 GHz CPU, 32 GB of memory, and an NVIDIA Quadro P4000 GPU. Table I displays the elapsed wall-clock times, per batch size, for 3D point cloud compression and decompression. Note that due to the parallel processing capability of the GPU, compression and decompression in larger batch sizes takes less time per point cloud.

#### B. Reconstruction Evaluation

Measuring the reconstruction capability of our model is crucial to evaluating its performance. However, direct quantitative comparisons between two point clouds is complicated by the property that the set of points comprising a point cloud is invariant to permutations. To address this issue, we utilized the chamfer distance (CD) [52] and earth mover's distance (EMD) [53]. The CD and EMD are two permutation-invariant metrics for comparing sets of points introduced in [54].

Initially, we used the same metrics (CD and EMD) to calculate the reconstruction loss and to train our model. Table II establishes a benchmark on the ShapeNet dataset using the CD, EMD, and  $F$ -score metrics. Despite the fact that both of the losses are differentiable almost everywhere, the CD is more efficient to compute in comparison to the EMD. In our experiments, we found that the training process converges faster when using the CD compared to the EMD. Notwithstanding, the EMD metric produces slightly higher-fidelity qualitative reconstruction results as shown in Fig. 3.

In a second experiment, we measured the performance of our network against Draco 1.4.1 [55], a state-of-the-art open-source library for compressing and decompressing 3D geometric meshes and point clouds. For this experiment,

Category	CD ( $\times 10^{-2}$ ) ↓			EMD ( $\times 10^{-2}$ ) ↓			F-score ↑		
	1.69 bpp	0.35 bpp	0.03 bpp	1.69 bpp	0.35 bpp	0.03 bpp	1.69 bpp	0.35 bpp	0.03 bpp
Airplane	0.063	0.068	0.074	2.041	2.361	2.170	0.995	0.995	0.992
Bag	0.343	0.362	0.392	2.733	3.346	2.439	0.788	0.764	0.744
Cap	0.550	0.600	0.595	2.386	2.298	3.151	0.652	0.591	0.623
Car	0.230	0.255	0.257	3.032	2.394	2.837	0.891	0.884	0.870
Chair	0.202	0.211	0.273	2.575	2.673	3.016	0.919	0.913	0.879
Earphone	0.463	0.457	0.656	3.237	2.192	2.822	0.762	0.784	0.735
Guitar	0.055	0.056	0.067	1.846	1.815	2.406	0.990	0.990	0.986
Knife	0.072	0.070	0.086	1.408	1.901	1.963	0.987	0.989	0.983
Lamp	0.321	0.349	0.389	2.274	3.054	3.091	0.845	0.826	0.807
Laptop	0.127	0.132	0.165	2.313	2.535	2.566	0.987	0.985	0.977
Motorbike	0.256	0.280	0.292	2.501	3.085	2.444	0.868	0.857	0.848
Mug	0.369	0.407	0.453	2.446	2.305	2.239	0.726	0.694	0.623
Pistol	0.110	0.128	0.138	2.611	2.276	2.206	0.974	0.970	0.963
Rocket	0.162	0.156	0.173	2.072	2.481	2.314	0.917	0.921	0.911
Skateboard	0.174	0.197	0.203	2.050	2.477	2.648	0.941	0.933	0.930
Table	0.179	0.195	0.230	2.039	2.475	2.690	0.934	0.923	0.903
Mean	0.230	0.245	0.278	2.347	2.479	2.562	0.886	0.876	0.861

TABLE II

RECONSTRUCTION LOSS VIA THE CHAMFER DISTANCE (CD) AND EARTH MOVER’S DISTANCE (EMD) ACROSS A RANGE OF BITS PER POINT (BPP) FOR EACH OBJECT CATEGORY IN THE SHAPENET [49] DATASET. THE F-SCORE WAS CALCULATED AT A DISTANCE THRESHOLD OF  $d = 0.05$ .

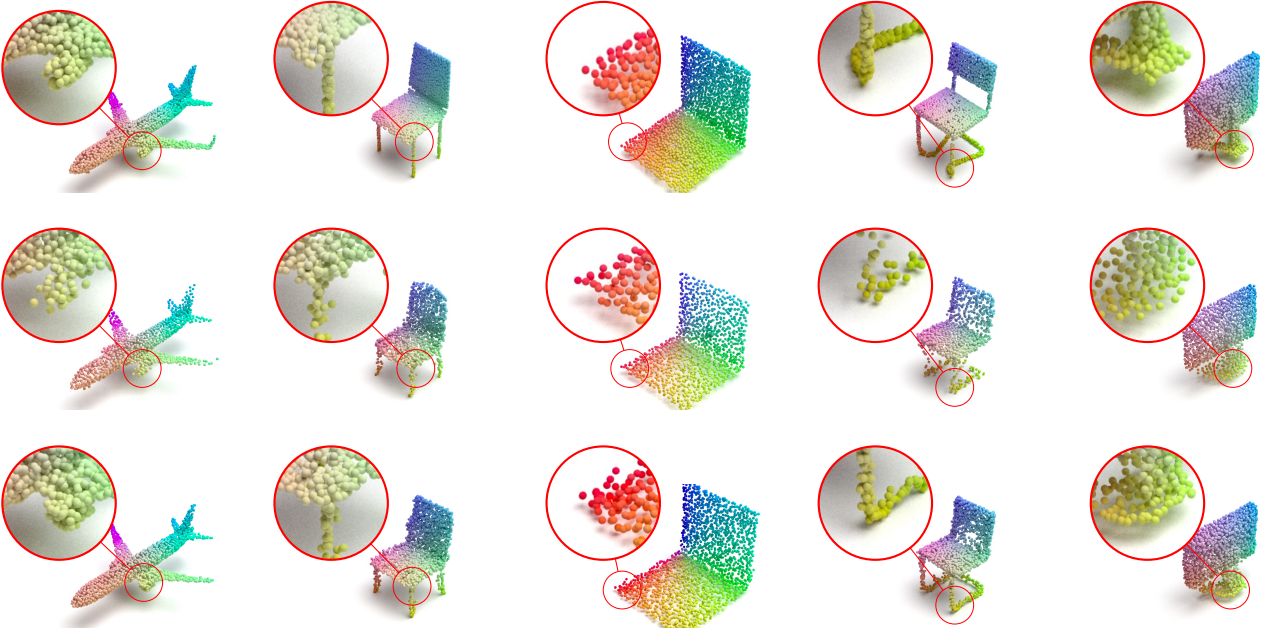


Fig. 3. The reconstruction results for a subset of objects from the ShapeNet [49] dataset. The first row shows the ground-truth point clouds. The second and third rows display the reconstructed point clouds using the chamfer distance and earth mover’s distance, respectively.

we again used ShapeNet and trained our model using the CD loss. The comparison was done using the point-to-point and point-to-surface distance metrics. These metrics are widely used to quantify 3D surface reconstruction quality and are described in [56]. Fig. 5 shows that our architecture outperforms Draco, especially at lower bitrates.

### C. Task-Specific Evaluation

An important and practical use case of compressed point cloud data is to store large amounts of 3D models and then preprocess them later on for downstream functions. To quantify the reconstruction quality of such tasks, we used

a PointNet [43] model to classify point cloud objects from ModelNet40. In this experiment, we trained a model using uncompressed data and determined its initial accuracy. Then, we used the trained model to classify the decompressed data and examined its accuracy against the original data. Note that both the uncompressed and decompressed data were compared using the same metric (e.g., CD or EMD).

Fig. 4 shows that our compression method preserves the semantic structure of the objects, even at low bitrates, while training with different loss functions. We can achieve similar accuracy with the CD metric on the compressed data (86%) when compared against the actual data (88%). An interesting



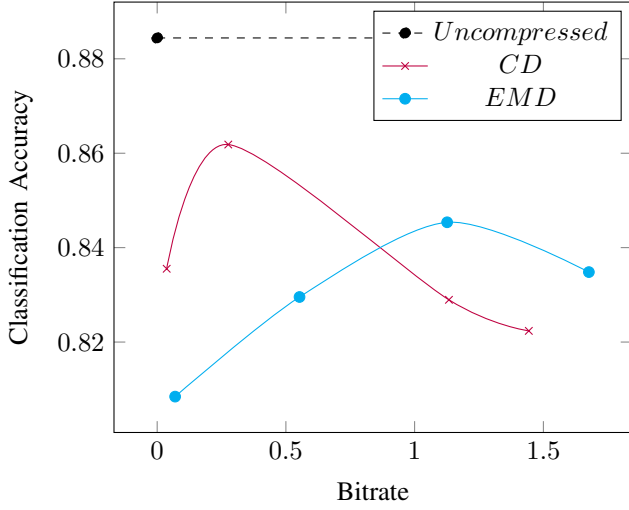


Fig. 4. A comparison of the classification accuracy for uncompressed and decompressed point cloud data using the chamfer distance (CD) and earth mover’s distance (EMD).

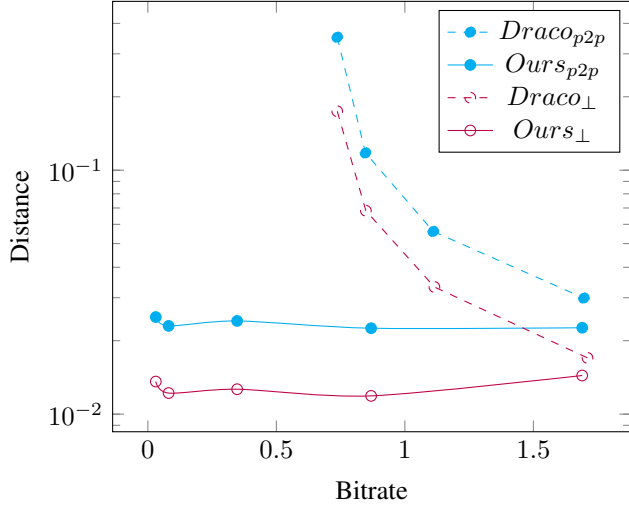


Fig. 5. The reconstruction quality of objects from the ShapeNet [49] dataset in terms of the point-to-point (p2p) and point-to-surface ( $p_{\perp}$ ) distances at different bitrates.

observation from this experiment is that the classification accuracy increases gradually with the bitrate, up to a certain optimal point, and then decreases. Based on these results, we hypothesize that the bitrate constraint acts as a regularizer that helps the model to better generalize.

#### D. Variable Bitrate Evaluation

This experiment showcases the possibility of using a single trained model to compress point cloud data at varying bitrates. At training time, the weighted entropy loss function (3) penalizes the lower-indexed vector elements more during the compression process. Consequently, this ensures that the high-frequency information is carried through the higher-indexed vector elements while the lower-indexed vector elements carry the overall shape information. The exponential decaying function (4) is used for assigning a weight to each

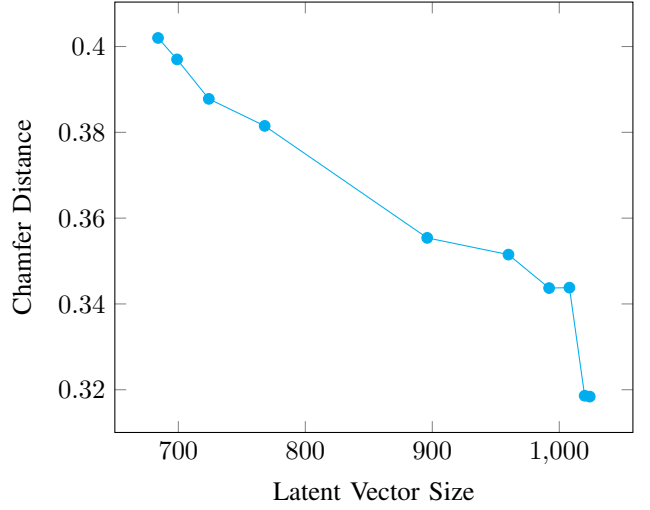


Fig. 6. The increase in reconstruction loss using a truncated latent vector to enable variable bitrates.

vector element where  $\omega_i$  is the  $i$ -th element in the weight vector.

For this experiment our model was trained using the CD metric, and the values 15 and 0.003 for variables  $a$  and  $b$ , respectively, were used for (4). At test time, we truncate the latent vector according to the bitrate setting and only compress the truncated vector instead of the whole vector. In Fig. 6, we illustrate the relationship between the loss and the number of vector elements used in the reconstruction. As we truncate the higher-indexed vector elements the distance between the actual and compressed point cloud gradually increases. This naturally results in a less accurate reconstruction.

#### V. CONCLUSION AND FUTURE WORK

We presented a deep learning-based approach that is capable of variable rate raw point cloud compression. Variable-rate compression is enabled by a tunable loss function that distributes information non-uniformly among the latent vector elements. This method alleviates the need for the training and storage of multiple models over a range of bitrates. The efficacy of our model was shown through the analysis of different components and the presentation of an extensive evaluation on the individual impact of these factors. What’s more, we established new benchmarks on publicly available datasets and we showed that our model surpasses state-of-the-art open-source software for compressing and decompressing 3D point clouds. In future work, we will investigate extending the range of bitrates a single model can support.

#### ACKNOWLEDGMENTS

The authors acknowledge the Texas Advanced Computing Center (TACC) at the University of Texas at Austin for providing software, computational, and storage resources that have contributed to the research results reported within this paper.

## REFERENCES

- [1] Z. Cai, J. Han, L. Liu, and L. Shao, "Rgb-d datasets using microsoft kinect or similar sensors: a survey," *Multimedia Tools and Applications*, vol. 76, no. 3, pp. 4313–4355, 2017.
- [2] Y. Guo, H. Wang, Q. Hu, H. Liu, L. Liu, and M. Bennamoun, "Deep learning for 3d point clouds: A survey," *IEEE Transactions on Pattern Analysis and Machine Intelligence*, 2020.
- [3] K. Sugimoto, R. A. Cohen, D. Tian, and A. Vetro, "Trends in efficient representation of 3d point clouds," in *Proceedings of the Asia-Pacific Signal and Information Processing Association Annual Summit and Conference*. IEEE, 2017, pp. 364–369.
- [4] C. Cao, M. Preda, and T. Zaharia, "3d point cloud compression: A survey," in *Proceedings of the International Conference on 3D Web Technology*, 2019, pp. 1–9.
- [5] W. J. Beksi and N. Papanikolopoulos, "Point cloud culling for robot vision tasks under communication constraints," in *Proceedings of the IEEE/RSJ International Conference on Intelligent Robots and Systems*, 2014, pp. 3747–3752.
- [6] M. I. Patel, S. Suthar, and J. Thakar, "Survey on image compression using machine learning and deep learning," in *Proceedings of the International Conference on Intelligent Computing and Control Systems*. IEEE, 2019, pp. 1103–1105.
- [7] <https://github.com/robotic-vision-lab/Variable-Rate-Compression-For-Raw-3D-Point-Clouds>.
- [8] D. Meagher, "Geometric modeling using octree encoding," *Computer Graphics and Image Processing*, vol. 19, no. 2, pp. 129–147, 1982.
- [9] Y. Huang, J. Peng, C.-C. J. Kuo, and M. Gopi, "Octree-based progressive geometry coding of point clouds," in *Proceedings of the Symposium on Point-Based Graphics*, vol. 6, 2006, pp. 103–110.
- [10] R. Schnabel and R. Klein, "Octree-based point-cloud compression," in *Proceedings of the Symposium on Point-Based Graphics*, vol. 6, 2006, pp. 111–120.
- [11] J. Kammerl, N. Blodow, R. B. Rusu, S. Gedikli, M. Beetz, and E. Steinbach, "Real-time compression of point cloud streams," in *Proceedings of the IEEE International Conference on Robotics and Automation*, 2012, pp. 778–785.
- [12] J. Elseberg, D. Borrmann, and A. Nüchter, "One billion points in the cloud—an octree for efficient processing of 3d laser scans," *ISPRS Journal of Photogrammetry and Remote Sensing*, vol. 76, pp. 76–88, 2013.
- [13] A. Hornung, K. M. Wurm, M. Bennewitz, C. Stachniss, and W. Burgard, "Octomap: An efficient probabilistic 3d mapping framework based on octrees," *Autonomous Robots*, vol. 34, no. 3, pp. 189–206, 2013.
- [14] R. Mekuria, K. Blom, and P. Cesar, "Design, implementation, and evaluation of a point cloud codec for tele-immersive video," *IEEE Transactions on Circuits and Systems for Video Technology*, vol. 27, no. 4, pp. 828–842, 2016.
- [15] J. L. Bentley, "Multidimensional binary search trees used for associative searching," *Communications of the ACM*, vol. 18, no. 9, pp. 509–517, 1975.
- [16] D. Cheriton and R. E. Tarjan, "Finding minimum spanning trees," *SIAM Journal on Computing*, vol. 5, no. 4, pp. 724–742, 1976.
- [17] P.-M. Gandoin and O. Devillers, "Progressive lossless compression of arbitrary simplicial complexes," *ACM Transactions on Graphics*, vol. 21, no. 3, pp. 372–379, 2002.
- [18] S. Gumhold, Z. Kami, M. Isenburg, and H.-P. Seidel, "Predictive point-cloud compression," in *ACM SIGGRAPH 2005 Sketches*, 2005.
- [19] B. Merry, P. Marais, and J. Gain, "Compression of dense and regular point clouds," in *Proceedings of the International Conference on Computer Graphics, Virtual Reality, Visualisation and Interaction in Africa*, 2006, pp. 15–20.
- [20] V. Zakharchenko, "Algorithm description of mpeg-pcc-tmc2," in *ISO/IEC JTC1/SC29/WG11/N17767*, 2018.
- [21] S. Schwarz, M. Preda, V. Baroncini, M. Budagavi, P. Cesar, P. A. Chou, R. A. Cohen, M. Krivokuća, S. Lasserre, Z. Li *et al.*, "Emerging mpeg standards for point cloud compression," *IEEE Journal on Emerging and Selected Topics in Circuits and Systems*, vol. 9, no. 1, pp. 133–148, 2018.
- [22] R. B. Rusu and S. Cousins, "3d is here: Point cloud library (pcl)," in *Proceedings of the IEEE International Conference on Robotics and Automation*, 2011, pp. 1–4.
- [23] T. Ochotta and D. Saupe, "Compression of point-based 3d models by shape-adaptive wavelet coding of multi-height fields," in *Proceedings of the Symposium on Point-Based Graphics*. The Eurographics Association, 2004.
- [24] P. Merkle, A. Smolic, K. Muller, and T. Wiegand, "Multi-view video plus depth representation and coding," in *Proceedings of the IEEE International Conference on Image Processing*, vol. 1, 2007, pp. 1–201.
- [25] T. Golla and R. Klein, "Real-time point cloud compression," in *Proceedings of the IEEE/RSJ International Conference on Intelligent Robots and Systems*, 2015, pp. 5087–5092.
- [26] L. He, W. Zhu, and Y. Xu, "Best-effort projection based attribute compression for 3d point cloud," in *Proceedings of the Asia-Pacific Conference on Communications*. IEEE, 2017, pp. 1–6.
- [27] X. Sun, H. Ma, Y. Sun, and M. Liu, "A novel point cloud compression algorithm based on clustering," *IEEE Robotics and Automation Letters*, vol. 4, no. 2, pp. 2132–2139, 2019.
- [28] C. Tu, E. Takeuchi, A. Carballo, and K. Takeda, "Point cloud compression for 3d lidar sensor using recurrent neural network with residual blocks," in *Proceedings of the IEEE International Conference on Robotics and Automation*, 2019, pp. 3274–3280.
- [29] G. K. Wallace, "The jpeg still picture compression standard," *IEEE Transactions on Consumer Electronics*, vol. 38, no. 1, pp. xviii–xxxiv, 1992.
- [30] G. J. Sullivan, J.-R. Ohm, W.-J. Han, and T. Wiegand, "Overview of the high efficiency video coding (hevc) standard," *IEEE Transactions on Circuits and Systems for Video Technology*, vol. 22, no. 12, pp. 1649–1668, 2012.
- [31] K. Ainala, R. N. Mekuria, B. Khathariya, Z. Li, Y.-K. Wang, and R. Joshi, "An improved enhancement layer for octree based point cloud compression with plane projection approximation," in *Proceedings of the Applications of Digital Image Processing*, vol. 9971. International Society for Optics and Photonics, 2016, pp. 223–231.
- [32] J. Wang, H. Zhu, Z. Ma, T. Chen, H. Liu, and Q. Shen, "Learned point cloud geometry compression," *arXiv preprint arXiv:1909.12037*, 2019.
- [33] A. F. Guarda, N. M. Rodrigues, and F. Pereira, "Deep learning-based point cloud geometry coding: Rd control through implicit and explicit quantization," in *Proceedings of the IEEE International Conference on Multimedia & Expo Workshops*, 2020, pp. 1–6.
- [34] F. Mentzer, E. Agustsson, M. Tschannen, R. Timofte, and L. Van Gool, "Conditional probability models for deep image compression," in *Proceedings of the IEEE Conference on Computer Vision and Pattern Recognition*, 2018, pp. 4394–4402.
- [35] A. F. Guarda, N. M. Rodrigues, and F. Pereira, "Deep learning-based point cloud coding: A behavior and performance study," in *Proceedings of the European Workshop on Visual Information Processing*. IEEE, 2019, pp. 34–39.
- [36] —, "Point cloud coding: Adopting a deep learning-based approach," in *Proceedings of the Picture Coding Symposium*. IEEE, 2019, pp. 1–5.
- [37] M. Quach, G. Valenzise, and F. Dufaux, "Learning convolutional transforms for lossy point cloud geometry compression," in *Proceedings of the IEEE International Conference on Image Processing*, 2019, pp. 4320–4324.
- [38] —, "Improved deep point cloud geometry compression," in *Proceedings of the IEEE International Workshop on Multimedia Signal Processing*, 2020, pp. 1–6.
- [39] L. Wiesmann, A. Milioto, X. Chen, C. Stachniss, and J. Behley, "Deep compression for dense point cloud maps," *IEEE Robotics and Automation Letters*, vol. 6, no. 2, pp. 2060–2067, 2021.
- [40] E. Agustsson, F. Mentzer, M. Tschannen, L. Cavigelli, R. Timofte, L. Benini, and L. Van Gool, "Soft-to-hard vector quantization for end-to-end learning compressible representations," *arXiv preprint arXiv:1704.00648*, 2017.
- [41] J. Ballé, V. Laparra, and E. P. Simoncelli, "End-to-end optimization of nonlinear transform codes for perceptual quality," in *Proceedings of the IEEE Picture Coding Symposium*, 2016, pp. 1–5.
- [42] L. Theis, W. Shi, A. Cunningham, and F. Huszár, "Lossy image compression with compressive autoencoders," *arXiv preprint arXiv:1703.00395*, 2017.
- [43] C. R. Qi, H. Su, K. Mo, and L. J. Guibas, "Pointnet: Deep learning on point sets for 3d classification and segmentation," in *Proceedings of the IEEE Conference on Computer Vision and Pattern Recognition*, 2017, pp. 652–660.

- [44] N. Ahmed, T. Natarajan, and K. R. Rao, "Discrete cosine transform," *IEEE Transactions on Computers*, vol. 100, no. 1, pp. 90–93, 1974.
- [45] J. Ballé, D. Minnen, S. Singh, S. J. Hwang, and N. Johnston, "Variational image compression with a scale hyperprior," *arXiv preprint arXiv:1802.01436*, 2018.
- [46] Y. Choi, M. El-Khamy, and J. Lee, "Variable rate deep image compression with a conditional autoencoder," in *Proceedings of the IEEE/CVF International Conference on Computer Vision*, 2019, pp. 3146–3154.
- [47] C. R. Qi, L. Yi, H. Su, and L. J. Guibas, "Pointnet++: Deep hierarchical feature learning on point sets in a metric space," *arXiv preprint arXiv:1706.02413*, 2017.
- [48] J. Rissanen and G. Langdon, "Universal modeling and coding," *IEEE Transactions on Information Theory*, vol. 27, no. 1, pp. 12–23, 1981.
- [49] A. X. Chang, T. Funkhouser, L. Guibas, P. Hanrahan, Q. Huang, Z. Li, S. Savarese, M. Savva, S. Song, H. Su *et al.*, "Shapenet: An information-rich 3d model repository," *arXiv preprint arXiv:1512.03012*, 2015.
- [50] Z. Wu, S. Song, A. Khosla, F. Yu, L. Zhang, X. Tang, and J. Xiao, "3d shapenets: A deep representation for volumetric shapes," in *Proceedings of the IEEE Conference on Computer Vision and Pattern Recognition*, 2015, pp. 1912–1920.
- [51] D. P. Kingma and J. Ba, "Adam: A method for stochastic optimization," *arXiv preprint arXiv:1412.6980*, 2014.
- [52] H. Barrow, J. Tenenbaum, R. Bolles, and H. Wolf, "Parametric correspondence and chamfer matching: Two new techniques for image matching," in *Proceedings of the Image Understanding Workshop*. Science Applications, Inc Arlington, VA, 1977, pp. 21–27.
- [53] Y. Rubner, C. Tomasi, and L. J. Guibas, "The earth mover's distance as a metric for image retrieval," *International Journal of Computer Vision*, vol. 40, no. 2, pp. 99–121, 2000.
- [54] H. Fan, H. Su, and L. J. Guibas, "A point set generation network for 3d object reconstruction from a single image," in *Proceedings of the IEEE conference on Computer Vision and Pattern Recognition*, 2017, pp. 605–613.
- [55] Google, *Draco 3D Data Compression*, 2021, <https://google.github.io/draco/>.
- [56] D. Tian, H. Ochimizu, C. Feng, R. Cohen, and A. Vetro, "Geometric distortion metrics for point cloud compression," in *Proceedings of the IEEE International Conference on Image Processing*, 2017, pp. 3460–3464.